



HAL
open science

Evolution of plasmonic nanostructures under ultra-low-energy ion bombardment

Lionel Simonot, Florian Chabanais, Sophie Rousselet, Frédéric Pailloux,
Sophie Camelio, David Babonneau

► **To cite this version:**

Lionel Simonot, Florian Chabanais, Sophie Rousselet, Frédéric Pailloux, Sophie Camelio, et al.. Evolution of plasmonic nanostructures under ultra-low-energy ion bombardment. Applied Surface Science, 2021, 544, pp.148672. 10.1016/j.apsusc.2020.148672 . hal-03219947

HAL Id: hal-03219947

<https://hal.science/hal-03219947>

Submitted on 28 May 2021

HAL is a multi-disciplinary open access archive for the deposit and dissemination of scientific research documents, whether they are published or not. The documents may come from teaching and research institutions in France or abroad, or from public or private research centers.

L'archive ouverte pluridisciplinaire **HAL**, est destinée au dépôt et à la diffusion de documents scientifiques de niveau recherche, publiés ou non, émanant des établissements d'enseignement et de recherche français ou étrangers, des laboratoires publics ou privés.

Evolution of plasmonic nanostructures under ultra-low-energy ion bombardment

Lionel Simonot^{a,*}, Florian Chabanais^{a,1}, Sophie Rousselet^a, Frédéric Pailloux^a, Sophie Camelio^a, David Babonneau^{a,*}

^a*Institut Prime, Département Physique et Mécanique des Matériaux, UPR 3346 CNRS, Université de Poitiers, SP2MI, TSA 41123, Cedex 9, 86073 Poitiers, France*

Abstract

Metal nanostructures supported on a dielectric substrate possess unique plasmonic properties that are highly dependent on their morphologies. We show that such nanostructures can be modified upon exposure to an ultra-low-energy ion-beam bombardment (< 100 eV) near the sputtering threshold of the metal. This plasma treatment can be easily implemented in a vacuum deposition chamber and allows the achievement of morphologies, and therefore optical properties, that are difficult to achieve otherwise by physical vapor deposition. We present the effects obtained (i) on self-organized Ag nanoparticles with unidirectional orientation and bimodal distribution, and (ii) on Ag layers in the form of percolated, quasi-continuous or island thin films. Our results show that the plasmonic dichroism of self-organized assemblies can be tuned thanks to the preferential sputtering of the smaller particles associated with gradual erosion of the larger ones. Ion-induced modifications of percolated or quasi-continuous films lead to the formation of isolated tiny particles with areal densities smaller than $500 \mu\text{m}^{-2}$. In both cases, the duration of the ion bombardment makes it possible to finely control the desired structural and plasmonic modifications.

Keywords: Metal nanostructures, Plasmonics, Ion bombardment

1. Introduction

Metal nanostructures embedded in or supported on an insulating matrix feature remarkable optical responses through interaction with an external electromagnetic field, owing to the phenomenon of so-called “localized surface plasmon resonance” (LSPR). Depending on their morphology (size and shape), spatial organization, and local environment, LSPR excitation of nanoparticles or nanowires of noble metals indeed gives rise to strong absorption bands in the ultraviolet, visible, or near infrared spectral ranges that are not present in the bulk metal. Envisioning original technologies and applications in chemistry, physics, biology, and medicine with plasmonic nanostructures

therefore requires the ability to suitably control the wavelength and intensity of the LSPR, *i.e.* to design the nanostructures on a custom basis by high-throughput self-assembly methods.

A common deposition technique for obtaining nanoparticles or discontinuous thin films with tunable plasmonic properties consists in sputtering, evaporating or vaporizing metallic targets under high vacuum conditions. By this process, the growth of the metal on a dielectric surface generally proceeds through the nucleation of islands, which gradually expand and coalesce [1]. During the coalescence stage, the number of particles per unit area progressively decreases and their average volume (in-plane size and height) increases. Furthermore, since the lateral growth of the particles is faster than the vertical growth, they become flatter and flatter as the deposition progresses. Coalescence continues by causing the particles to elongate in the plane, and to get closer to each other, until percolation is reached. The remaining pores are then filled to eventually form a continuous metal film with

*Corresponding authors

Email addresses: lionel.simonot@univ-poitiers.fr (Lionel Simonot), david.babonneau@univ-poitiers.fr (David Babonneau)

¹Now at Normandie Univ, UNIROUEN, INSA Rouen, CNRS, Groupe de Physique des Matériaux, 76000 Rouen, France.

rough surface. Although the resulting plasmonic properties are extremely sensitive to this evolution of the metal nanostructure, the growth process that is mediated by kinetically driven mechanisms limits the range of possibilities. This makes it difficult to independently control the size, shape and areal density of nanoparticles. In particular, assemblies of “densely-packed” nanoparticles that present a short-range order and a bimodal distribution of morphologies are often obtained. To overcome this difficulty, it is usually worthwhile to carry out treatments during or after deposition. While thermal annealing is probably the most common approach, plasma and ion-beam treatments represent promising alternatives worthy of exploration [2–8]. Ion-beam effects on nanostructured thin films are highly dependent on ion energy. For energy greater than hundreds of keV, irradiation and implantation can occur that enables buried nanoparticles to be deformed by ion-beam-shaping process [9–11]. At these energies, ion irradiation can also modify arrays of supported nanoparticles [12, 13], or induce the formation of nanoparticles by dewetting of continuous thin films [14, 15]. At hundreds of eV, ion bombardment results in the removal of atoms from the surface and can be used as an effective method for surface etching or cleaning [16, 17], but also for creating periodic patterns of dots or ripples on metallic surfaces [18–20], or for modifying island thin films [21, 22]. An advantage of such plasma and ion-beam treatments is their easy incorporation into high vacuum systems [17] and their high fabrication throughput over cm^2 scale areas. Indeed, ion bombardment with a broad beam can be fairly easily implemented in the same setup as the one used for thin film deposition by directing the ion flow towards the substrate. However, at energies greater than 200 eV, many adverse effects are commonly observed such as ion-beam mixing or amorphization [12, 16, 22, 23]. To limit the deleterious impact of these radiation damages, we focus on ion energy below 100 eV, *i.e.* near or just above the sputtering threshold of the metal, and we investigate the influence of the initial morphology of the nanostructured metal film. First, we present the effect of ultra-low-energy Ar^+ -ion bombardment on self-organized Ag nanoparticles with bimodal distribution grown by glancing-angle ion-beam sputtering deposition on nanorippled alumina surfaces. We then report on the evolution of percolated, quasi-continuous and island Ag layers fabricated by magnetron sputtering deposition on Si_3N_4 buffer-layers.

2. Experimental details

2.1. Sample preparation

Self-organized nanoparticle chains. Self-organized Ag nanoparticles with bimodal distribution were obtained using a NordikoTM dual ion-beam chamber following a four-step sequence under high vacuum ($\sim 4 \times 10^{-8}$ mbar base pressure), which is explained in detail in Refs. [24] and [25]. In short, amorphous layers of alumina were first deposited at room temperature on two-side polished fused silica and on NaCl single crystals, followed by 1 keV Xe^+ -ion etching at a sputtering angle of $\vartheta = 55^\circ$ with respect to the surface normal and a total fluence of about 5.4×10^{17} ions cm^{-2} , leading to the formation of periodic patterns consisting of unidirectional ripples oriented in the direction perpendicular to the projection of the ion beam (see Fig. S1). Self-aligned chains of Ag nanoparticles were then obtained by depositing a small amount of metal (effective thickness of 2.4 nm) under a grazing incidence of 2° from the mean surface, thus ensuring replication of the ripple pattern by shadowing effects. Low-energy Ar^+ -ion bombardment at 80 eV was finally applied directly to the Ag nanostructures at normal incidence ($\vartheta = 0^\circ$) with a flux of about 3×10^{15} ions $\text{cm}^{-2} \text{s}^{-1}$, before deposition of an alumina capping-layer totaling 12 nm in thickness to provide optimal protection for the nanoparticles against ageing before *post mortem* structural and optical characterizations.

Quasi-continuous, percolated, and island layers. In order to investigate the ion-induced structural and optical changes of quasi-continuous, percolated, and island Ag layers, 10-nm thick amorphous layers of Si_3N_4 were first deposited at room temperature by reactive magnetron sputtering on one-side polished glass substrates and on NaCl single crystals. Deposition of Ag (effective thickness of 12.8 nm, 8.0 nm, and 3.2 nm) was then accomplished onto these unrippled Si_3N_4 buffer-layers at a glancing angle of $\vartheta = 25^\circ$ with respect to the surface normal, before a delay time of 600 s followed by exposure to 80 eV Ar^+ -ion bombardment at normal incidence. The resulting Ag nanostructures were finally capped with a protective 12-nm thick layer of Si_3N_4 .

2.2. Characterization methods

The nanostructured Ag thin films were analyzed by transmission electron microscopy (TEM) with a

JEOL 2200FS microscope fitted with an in-column Ω -filter and a Schottky field emission gun operated at 200 kV. Prior to the observation, free-standing films deposited on NaCl single crystals were transferred onto copper grids after dissolving the substrate in purified water. Direct imaging was carried out from plane views by high-angle annular dark-field scanning TEM (HAADF-STEM) with a probe size of 0.7 nm. Diffraction patterns were also acquired by employing energy filtered selected area electron diffraction (EF-SAED).

The macroscopic optical response of the samples with self-organized nanoparticles was investigated by means of spectroscopic transmission using a Cary 5000 spectrophotometer from Agilent Technologies equipped with a rotating polarizer. *Post mortem* transmittance measurements were performed at normal incidence (beam diameter ~ 3 mm) in the spectral range between 250 nm and 2000 nm using longitudinal (\parallel) or transverse (\perp) polarization with respect to the ripple direction. In addition to experimental measurements, numerical simulations were performed by finite-difference time-domain (FDTD) calculations using the FDTD Solutions software purchased from Lumerical [26]. Regarding the quasi-continuous, percolated, and island layers grown by magnetron sputtering deposition, *in situ* monitoring of the optical response was carried out in real time during both deposition and plasma treatment by surface differential reflectance spectroscopy (SDRS), using the setup described in Ref. [27]. The sample was illuminated using s-polarized white light at an angle of 70° to the surface normal. The reflected intensity was collected in the specular direction by a spectrophotometer at a rate of one spectrum per second within the spectral range 350–950 nm. The reflectance R_0 just before Ag deposition is taken as a reference.

3. Results and discussion

3.1. Self-organized Ag nanoparticle chains

Figure 1(a) shows plane-view images taken by HAADF-STEM for self-organized Ag nanoparticles grown on rippled alumina thin films. The top row displays the results obtained for a sample that was not subjected to ion bombardment before capping-layer deposition. HAADF-STEM clearly reveals a bimodal distribution of individual nanoparticles with two groups exhibiting different sizes and morphologies. Careful analysis has been

Table 1: Morphological parameters retrieved from the analysis of HAADF-STEM images acquired on self-organized Ag nanoparticles grown on rippled alumina thin films and subjected to 80 eV Ar⁺-ion bombardment at normal incidence before alumina capping-layer deposition: duration of the ion-bombardment treatment (t_{sput}), areal density of nanoparticles (d), coverage rate (τ), average in-plane diameters in the longitudinal (D_{\parallel}) and transverse (D_{\perp}) directions with the corresponding standard deviations (σ_{\parallel} and σ_{\perp}), and average interparticle gaps in the longitudinal direction (\bar{g}) with the corresponding standard deviations (σ_g).

$\sqrt{D_{\parallel}D_{\perp}}$	t_{sput} (s)	0	60	120
> 1.5 nm	d (μm^{-2})	4230	1770	1880
	τ (%)	33.9	30.6	22.7
> 9.0 nm	d (μm^{-2})	1090	960	1340
	τ (%)	30.1	29.1	21.7
	D_{\parallel} (nm)	28.1	27.8	18.1
	σ_{\parallel} (nm)	18.2	17.7	8.9
	D_{\perp} (nm)	13.0	14.3	11.6
	σ_{\perp} (nm)	2.5	2.2	1.5
	\bar{g} (nm)	5.4	6.9	8.4
σ_g (nm)	4.6	5.3	4.2	

accomplished by digital image processing assuming ellipsoidal nanoparticles with in-plane diameters D_{\parallel} and D_{\perp} in the longitudinal and transverse directions, respectively (Table 1). It is worth noting that, as a result of shadowing effects and inhomogeneous anisotropic coalescence in the zones illuminated by the metal flux during Ag deposition [24, 25], the larger nanoparticles (effective diameter $\sqrt{D_{\parallel}D_{\perp}} > 9.0$ nm) are predominantly elongated and aligned along the underlying ripples, thus forming linear chains spaced about 28 nm apart in the transverse direction, *i.e.*, approaching the periodicity of the pre-patterned alumina surface. By comparison, the smaller particles located between the chains are more circular on average. The bimodal nature is very marked on the D_{\parallel} and D_{\perp} histograms [Fig. 1(b)] which, in addition, highlight a much broader size distribution of the large particles in the longitudinal direction. As shown in Fig. 1(c), there is also a certain distribution of gaps between adjacent particles with an average value of $\bar{g} = 5.4$ nm (standard deviation of $\sigma_g = 4.6$ nm) and a high density of narrow gaps smaller than 5 nm, which is a key determining factor to promote spectral red-shift of the LSPR together with strong increase of the near-field intensity at the LSPR wavelength. Hence, absorbance

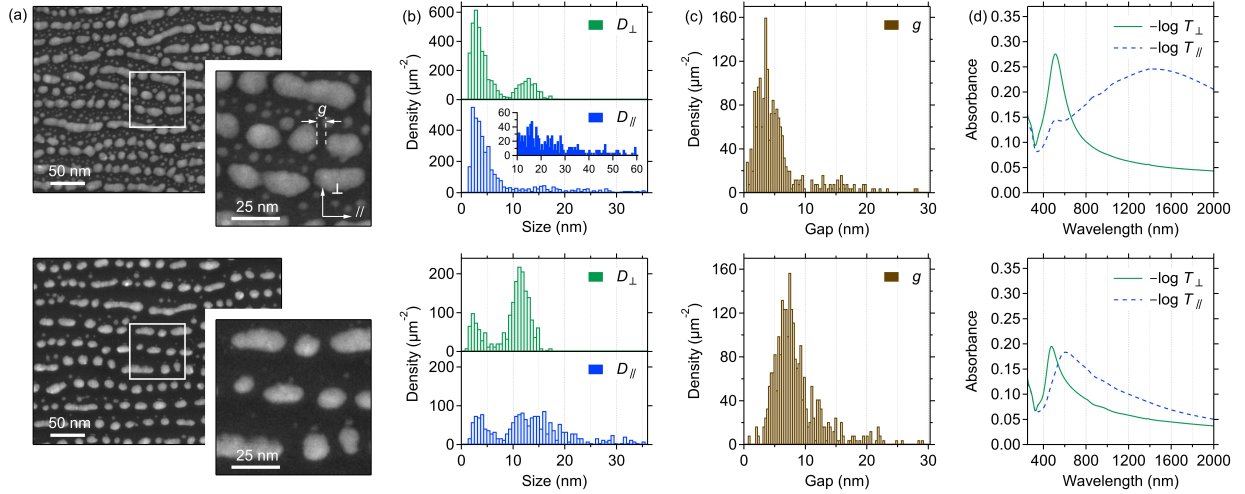


Figure 1: Self-organized Ag nanoparticles grown on rippled alumina thin films without (top) and with (bottom) 80 eV Ar⁺-ion bombardment at normal incidence for 120 s before alumina capping-layer deposition. (a) Plane-view HAADF-STEM images with zoomed areas indicated by the white rectangles, (b) in-plane size distributions in the transverse (D_{\perp}) and longitudinal (D_{\parallel}) directions, (c) distributions of interparticle gaps (g), and (d) corresponding absorbance spectra collected with transverse and longitudinal polarizations of the incident light.

215 spectra derived from transmittance measurements
 at normal incidence ($-\log T$), display a strong de-
 pendence on the polarization of the incident light
 with respect to the nanoparticle chains [Fig. 1(d)].
 As demonstrated from previous analytical calcula-
 220 tions and numerical simulations [24, 25], the opti-
 cal response of such systems can be related to their
 nanostructural properties. For a transverse polar-
 ization, the LSPR is located around 510 nm and
 is mainly due to the plasmonic response of individ-
 225 ual particles sufficiently distant from each other to
 consider electromagnetic interactions between par-
 ticles to be negligible. In contrast, for a longitudi-
 nal polarization, the LSPR is red-shifted to the near-
 infrared region and spreads over a wider spectral
 230 range. This behavior can obviously be explained
 by the effects of electromagnetic coupling between
 particles with large aspect ratios ($\overline{D_{\parallel}}/\overline{D_{\perp}} \approx 2.17$),
 but also by the broad size and gap distributions in
 the longitudinal direction (see FDTD calculations
 235 provided in the supplementary material for further
 details on the influence of the interparticle gap and
 of the in-plane diameter in the longitudinal direc-
 tion, Fig. S2). For completeness, it should be noted
 240 that a second resonance of low amplitude is present
 around 520 nm, mainly due to the smaller isolated
 and more spherical particles.

On the bottom row of Fig. 1 are presented the re-
 sults obtained for a sample that has undergone Ar⁺-

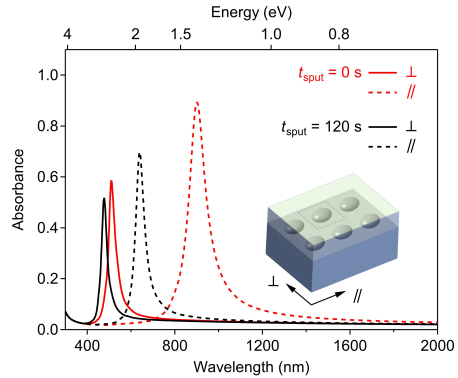


Figure 2: Absorption spectra calculated by FDTD method using the morphological parameters gathered in Table 1 for $t_{\text{sput}} = 0$ s ($H = 5.0$ nm) and $t_{\text{sput}} = 120$ s ($H = 6.2$ nm).

ion bombardment for 120 s (see also Table 1). In
 245 comparison with the untreated sample, the number
 of small nanoparticles ($\sqrt{D_{\parallel}D_{\perp}} < 9.0$ nm) predom-
 inantly located between the chains decreased signifi-
 cantly, a result which can be ascribed to a size-
 dependent sputtering yield [12, 22]. Concomitantly,
 250 the larger particles with anisotropic shape and uni-
 directional orientation have been eroded. As a conse-
 quence, the resonant particles are slightly smaller
 ($\approx -22\%$ in effective diameter) and less elongated
 overall ($\overline{D_{\parallel}}/\overline{D_{\perp}} \approx 1.56$). Also, for a transverse po-
 larization of the incident light, a blue-shifted reso-

nance around 480 nm is induced with a smaller amplitude because the total amount of Ag decreased. The effect is much more pronounced for a longitudinal polarization, with the LSPR now being at about 610 nm and much narrower than without ion bombardment. Furthermore, the low-amplitude resonance around 520 nm is no longer visible. These observations are consistent with the reduced variety of particle morphologies, but also with the 55% increase of the average gap between adjacent particles ($\bar{g} = 8.4$ nm with $\sigma_g = 4.2$ nm), thus causing less electromagnetic coupling. As shown in Fig. 2, such an evolution of the optical response can be qualitatively predicted by numerical simulations performed by FDTD calculations, with the height of the Ag nanoparticles, H , being adjusted in order to fit the experimental LSPR position for a transverse excitation. Numerical simulations in turn suggest that ion-induced reshaping also causes an increase of the out-of-plane aspect ratio, H/D_{\perp} , from ~ 0.38 to 0.53. In the end, the plasmonic dichroism of the assembly is still present but is significantly diminished. Details on an intermediate situation corresponding to an ion-bombardment duration of $t_{\text{sput}} = 60$ s are provided in the supplementary material (Fig. S3) and in Table 1, proving that low-energy ion bombardment makes it possible to finely tune the plasmonic dichroism of anisotropic metal nanostructures.

3.2. Quasi-continuous, percolated, and island Ag layers

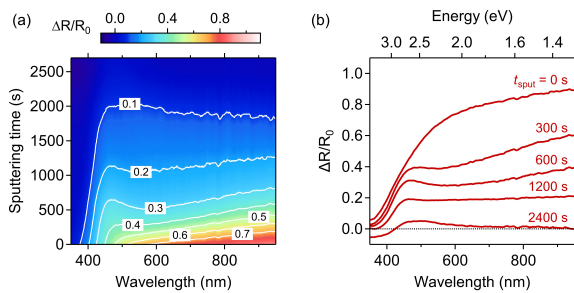


Figure 3: (a) Map of the SDRS signal $\Delta R(\lambda, t_{\text{sput}})/R_0$ collected during 80 eV Ar^+ -ion bombardment at normal incidence on an initially percolated Ag layer grown on a flat Si_3N_4 surface. (b) Corresponding SDRS spectra for different sputtering durations t_{sput} . $R(\lambda)$ is the film reflectance at time t_{sput} and $R_0(\lambda)$ is that of the 10-nm thick Si_3N_4 buffer-layer deposited on glass substrate being used as a reference.

Figure 3 shows the SDRS spectra collected under

s -polarized light during Ar^+ -ion bombardment of a percolated Ag layer (initial effective Ag thickness of 8.0 nm) grown by magnetron sputtering deposition on a flat Si_3N_4 buffer-layer. The optical response of the initial percolated Ag layer ($t_{\text{sput}} = 0$ s) shows an asymptotic behavior above 500 nm consistent with a random distribution of plasmonic eigenmodes over a broad spectral range due to the semi-continuous metal structure [28]. Upon exposure to ion bombardment, the signal gradually decreases leading to the emergence of a weak LSPR in the range of 470-500 nm after about 300 s. However, this resonance coexists with the quasi-metallic behavior of the layer at long wavelengths almost up to the very end of the bombardment. Finally, after about 40 minutes, the ion-bombarded $\text{Ag}:\text{Si}_3\text{N}_4$ bilayer becomes transparent at long wavelengths ($\Delta R/R_0 \rightarrow 0$) and the SDRS signal displays only the weak LSPR at about 500 nm. For comparison, SDRS spectra were also recorded during ion bombardment of a bare Si_3N_4 layer under identical conditions (Fig. S4). No significant change of the signal was observed for 3500 s, proving that Si_3N_4 sputtering is negligible. Such an evolution of optical properties can thus be closely related to ion-induced morphological changes of the percolated Ag layer [1, 11, 27], as evidenced through HAADF-STEM observations of $\text{Si}_3\text{N}_4:\text{Ag}:\text{Si}_3\text{N}_4$ trilayers presented in Fig. 4. During the first stages of low-energy Ar^+ -ion bombardment [Figs. 4(a)–4(c)], it can be seen that the coverage rate progressively decreases and percolating paths become slimmer, while the number of isolated particles increases and their average size decreases. After 20 minutes of exposure [Fig. 4(d)], relatively circular particles coexist with very elongated particles, residues of previous percolated structures. Nevertheless, after further ion bombardment [Fig. 4(e)], it is particularly noteworthy that all disconnected nanostructures are eventually transformed into quasi-circular nanoparticles, which appear to be very distant from each other. Moreover, both the average nanoparticle size and the corresponding size dispersion have significantly decreased [Fig. 4(f)], thereby enabling the development of plasmonic nanoparticles with average size of 8.2 nm (standard deviation of 3.0 nm) and interparticle distance as high as 44 nm on average. According to EF-SAED patterns (Fig. 5), randomly oriented Ag particles remain crystalline until the end of the treatment. Although slight interfacial mixing cannot be completely ruled out, these findings indicate that total

340 mixing or amorphization of Ag does not occur under ultra-low-energy ion bombardment.

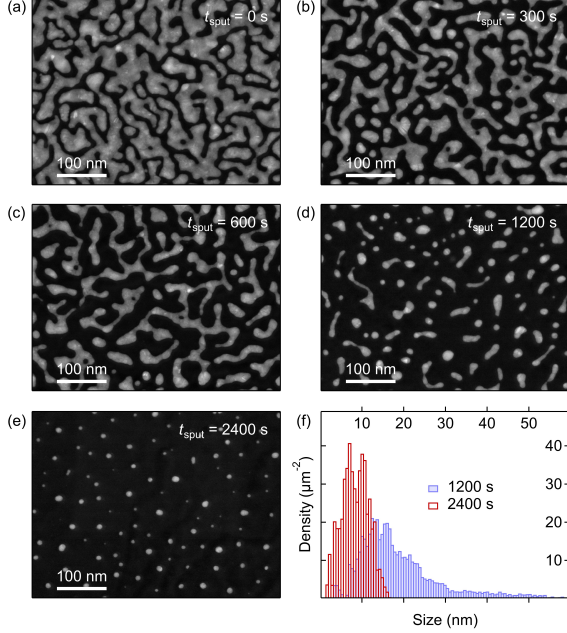


Figure 4: Plane-view HAADF-STEM images of $\text{Si}_3\text{N}_4:\text{Ag}:\text{Si}_3\text{N}_4$ trilayers corresponding to different sputtering durations t_{sput} of an initially percolated Ag layer subjected to 80 eV Ar^+ -ion bombardment at normal incidence. (a) $t_{\text{sput}} = 0$ s, (b) $t_{\text{sput}} = 300$ s, (c) $t_{\text{sput}} = 600$ s, (d) $t_{\text{sput}} = 1200$ s, (e) $t_{\text{sput}} = 2400$ s, and (f) nanoparticle size distributions after 1200 s and 2400 s of ion bombardment.

345 With the aim of comparing the evolution of different initial Ag nanostructures under ultra-low-energy Ar^+ -ion bombardment, similar plasma treatments were conducted with Ag layers corresponding to various growth stages: in addition to the percolating network previously described, we also considered a quasi-continuous film (12.8 nm effective thickness) and an assembly of coalescing nanoparticles with short-range order (3.2 nm effective thickness). Results presented in the supplementary material (Figs. S5–S8) show that the initially quasi-continuous Ag layer behaves like the percolated one, although with a different kinetics, which leads to the formation of well-separated individual nanoparticles with areal density of $\sim 460 \mu\text{m}^{-2}$ after 1500 s of ion bombardment. In contrast, for initially densely-packed coalescing nanoparticles, Ag sputtering associated with enhanced surface mobility of Ag adatoms results in a gradual increase of the areal density of nanoparticles from $\sim 3730 \mu\text{m}^{-2}$ ($t_{\text{sput}} = 0$ s) to \sim

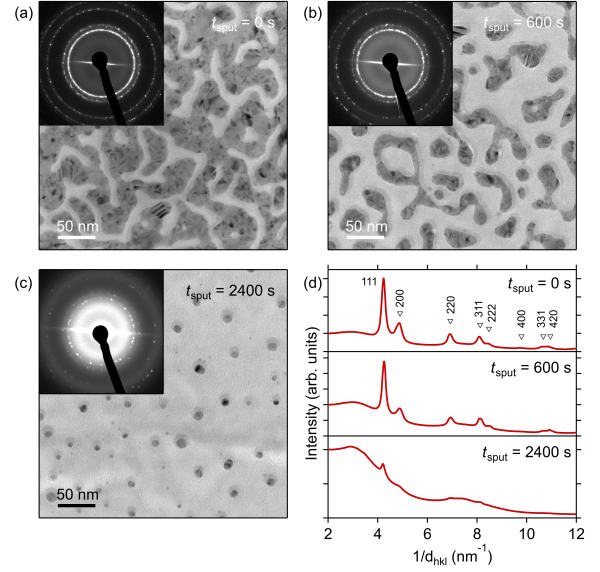


Figure 5: Plane-view energy filtered TEM images and EFSAED patterns for $\text{Si}_3\text{N}_4:\text{Ag}:\text{Si}_3\text{N}_4$ trilayers corresponding to different sputtering durations t_{sput} of an initially percolated Ag layer (8.0 nm effective thickness) subjected to 80 eV Ar^+ -ion bombardment at normal incidence. (a) $t_{\text{sput}} = 0$ s, (b) $t_{\text{sput}} = 600$ s, and (c) $t_{\text{sput}} = 2400$ s. (d) Corresponding electron diffraction averaged profiles together with the position of the main lines for Ag with face-centered cubic Fm3m structure.

365 $5510 \mu\text{m}^{-2}$ after 600 s of ion bombardment. The evolution of the Ag coverage rate τ as a function of the sputtering duration t_{sput} is presented in Fig. 6. Data were retrieved from the analysis of binarized plane-view HAADF-STEM images by measuring the surface fraction covered by Ag, and the total Ag sputtering duration corresponding to $\tau(t_{\text{sput}}) = 0$ was obtained from SDRS data, *i.e.* $\Delta R(t_{\text{sput}})/R_0 = 0$. Each experimental curve was fitted with an exponential function of the form $\tau(t_{\text{sput}}) = \tau_0(1 - \rho)^{t_{\text{sput}}}$, where $\tau_0 = \tau(0)$ and ρ is a parameter that relates to the sputtering yield of the Ag nanostructures. As expected, irrespective of the initial Ag nanostructure, the sputtering rate reduces progressively because the probability of Ar^+ -ion interaction with Ag atoms decreases as τ is diminished. However, while $\rho \approx 1.3 \times 10^{-3}$ for initially percolated or quasi-continuous Ag layers, it rises to $\rho \approx 2.1 \times 10^{-3}$ in the case of densely-packed coalescing nanoparticles. These findings suggest that the sputtering of Ag nanoparticles is significantly enhanced compared to percolated Ag films because of the higher specific surface area

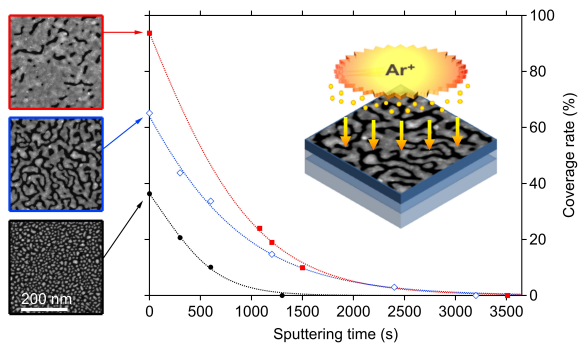


Figure 6: Evolution of the Ag coverage rate as a function of the sputtering duration for different initial Ag nanostructures subjected to 80 eV Ar^+ -ion bombardment at normal incidence. Dotted lines are fits to an exponential function of the form $\tau(t_{\text{sput}}) = \tau_0(1 - \rho)^{t_{\text{sput}}}$ specified by $\tau_0 = 93.7\%$ and $\rho = 1.34 \times 10^{-3}$ (red curve), $\tau_0 = 65.1\%$ and $\rho = 1.21 \times 10^{-3}$ (blue curve), and $\tau_0 = 36.4\%$ and $\rho = 2.11 \times 10^{-3}$ (black curve), respectively. Plane-view HAADF-STEM images of untreated $\text{Si}_3\text{N}_4:\text{Ag}:\text{Si}_3\text{N}_4$ trilayers are also shown to provide a vision of the initial Ag nanostructures with effective Ag thickness of 12.8 nm (top), 8.0 nm (middle), and 3.2 nm (bottom), respectively.

and lower volume to dissipate the primary ion energy [29–31]. In addition to these sputtering processes, it can be noted that universal mechanisms such as thermally-induced diffusion, viscous flow, and dewetting may also contribute to the evolution of the metallic nanostructures under ultra-low-energy ion bombardment [8].

4. Conclusions

In conclusion, we have shown that ultra-low-energy ion-beam bombardment of nanostructured Ag layers grown by physical vapor deposition significantly modifies the initial film. This plasma treatment near the sputtering threshold makes it possible to obtain various original nanostructures that are difficult or impossible to synthesize otherwise, and therefore opens the way for obtaining assemblies with unique properties. The observed effects depend on both the initial nanostructure and the ion-bombardment duration, while the ion energy should impact the kinetics of the observed phenomena [5]. The use of ultra-low-energy (< 100 eV) and chemically non-reactive ions preserves the dielectric substrate and the crystallinity of the Ag nanostructures. It also allows the fine tuning of the sputtering yield of Ag. As a consequence, depending on the initial nanostructure, the final areal

density of the assembly can be fully controlled so that the study of non-interacting or single particles can be considered [32–34]. Furthermore, such an approach could be an efficient means of plasmonic structural coloring [35]. This soft treatment can easily be integrated as an additional step in nanostructured film synthesis by physical vapor deposition in order to optimize the optical properties of the manufactured samples, also when using flexible substrates that degrade under high temperature conditions. Moreover, ion bombardment at oblique angles should provide an additional degree of freedom to selectively modify the shape of nanostructures.

Acknowledgements

The authors wish to acknowledge the technical support of Philippe Guérin in thin film deposition.

Supplementary material

See the supplementary material for atomic force microscopy of a nanorippled alumina surface obtained after 1 keV Xe^+ -ion exposure at oblique incidence (Fig. S1), numerical simulations performed by finite-difference time-domain calculations (Fig. S2), as well as HAADF-STEM images and absorbance spectra for self-organized Ag nanoparticles grown on a rippled alumina thin film after 80 eV Ar^+ -ion bombardment at normal incidence for 60 s (Fig. S3). Further SDRS spectra and/or HAADF-STEM images of a bare Si_3N_4 film (Fig. S4), quasi-continuous Ag layers (Figs. S5–S6), and coalescing Ag nanoparticles with short-range order (Figs. S7–S8) under ultra-low-energy Ar^+ -ion bombardment are also presented.

References

- [1] G. Abadias, L. Simonot, J. J. Colin, A. Michel, S. Camelio, D. Babonneau, Volmer-Weber growth stages of polycrystalline metal films probed by in situ and real-time optical diagnostics, *Appl. Phys. Lett.* 107 (2015) 183105.
- [2] X. Meng, T. Shibayama, R. Yu, J. Ishioka, S. Watanabe, Ion beam surface nanostructuring of noble metal films with localized surface plasmon excitation, *Curr. Opin. Solid State Mat. Sci.* 21 (2017) 177–188.
- [3] R. Lo Savio, L. Repetto, B. Šetina Batič, G. Firpo, U. Valbusa, Local nanostructuring of gold thin films through dewetting induced by Ga^+ irradiation, *Nucl. Instrum. Methods Phys. Res. Sect. B-Beam Interact. Mater. Atoms* 354 (2015) 129–133.

- [4] Y. Fang, B. Zhang, L. Hong, D. Yao, Z. Xie, Y. Jiang, Improvement of photocatalytic activity of silver nanoparticles by radio frequency oxygen plasma irradiation, *Nanotechnology* 26 (2015) 295204.
- [5] V. Antad, L. Simonot, D. Babonneau, Influence of low-energy plasma annealing on structural and optical properties of silver nanoclusters grown by magnetron sputtering deposition, *J. Nanopart. Res.* 16 (2014) 2328.
- [6] V. Antad, L. Simonot, D. Babonneau, Tuning the surface plasmon resonance of silver nanoclusters by oxygen exposure and low-energy plasma annealing, *Nanotechnology* 24 (2013) 045606.
- [7] M. I. Lapsley, A. Shahrvan, Q. Hao, B. K. Juluri, S. Giardinelli, M. Lu, Y. Zhao, I.-K. Chiang, T. Matsoukas, T. Jun Huang, Shifts in plasmon resonance due to charging of a nanodisk array in argon plasma, *Appl. Phys. Lett.* 100 (2012) 101903.
- [8] X. Zhou, Q. Wei, K. Sun, L. Wang, Formation of ultrafine uniform gold nanoparticles by sputtering and redeposition, *Appl. Phys. Lett.* 94 (2009) 133107.
- [9] F. Ren, C. Jiang, C. Liu, J. Wang, T. Oku, Controlling the morphology of Ag nanoclusters by ion implantation to different doses and subsequent annealing, *Phys. Rev. Lett.* 97 (2006) 165501.
- [10] G. Rizza, P. E. Coulon, V. Khomenkov, C. Dufour, I. Monnet, M. Toulemonde, S. Perruchas, T. Gacoin, D. Mailly, X. Lafosse, C. Ulysse, E. A. Dawi, Rational description of the ion-beam shaping mechanism, *Phys. Rev. B* 86 (2012) 035450.
- [11] J. Toudert, D. Babonneau, S. Camelio, T. Girardeau, F. Yubero, J. Espinós, A. R. González-Elipse, Using ion beams to tune the nanostructure and optical response of co-deposited Ag:BN thin films, *J. Phys. D: Appl. Phys.* 40 (2007) 4614–4620.
- [12] A. Klimmer, P. Ziemann, J. Biskupek, U. Kaiser, M. Flesch, Size-dependent effect of ion bombardment on Au nanoparticles on top of various substrates: thermodynamically dominated capillary forces versus sputtering, *Phys. Rev. B* 79 (2009) 155427.
- [13] F. Ruffino, R. De Bastiani, M. G. Grimaldi, C. Bongiorno, F. Giannazzo, F. Roccaforte, C. Spinella, V. Raineri, Self-organization of Au nanoclusters on the SiO₂ surface induced by 200 keV-Ar⁺ irradiation, *Nucl. Instrum. Methods Phys. Res. Sect. B-Beam Interact. Mater. Atoms* 257 (2007) 810–814.
- [14] J. Prakash, A. Tripathi, V. Rigato, J. C. Pivin, J. Tripathi, K. H. Chae, S. Gautam, P. Kumar, K. Asokan, D. K. Avasthi, Synthesis of Au nanoparticles at the surface and embedded in carbonaceous matrix by 150 keV Ar ion irradiation, *J. Phys. D: Appl. Phys.* 44 (2011) 125302.
- [15] X. Meng, T. Shibayama, R. Yu, S. Takayanagi, S. Watanabe, Microstructure analysis of ion beam-induced surface nanostructuring of thin Au film deposited on SiO₂ glass, *J. Mater. Sci.* 48 (2013) 920–928.
- [16] M. V. Ramana Murty, Sputtering: the material erosion tool, *Surf. Sci.* 500 (2002) 523–544.
- [17] E. Taglauer, Surface cleaning using sputtering, *Appl. Phys. A* 51 (1990) 238–251.
- [18] A. Toma, D. Chiappe, C. Boragno, F. Buatier de Mongeot, Self-organized ion-beam synthesis of nanowires with broadband plasmonic functionality, *Phys. Rev. B* 81 (2010) 165436.
- [19] M. V. Ramana Murty, T. Curcic, A. Judy, B. H. Cooper, A. R. Woll, J. D. Brock, S. Kycia, R. L. Headrick, X-ray scattering study of the surface morphology of Au (111) during Ar⁺ ion irradiation, *Phys. Rev. Lett.* 80 (1998) 4713.
- [20] D. Ghose, Ion beam sputtering induced nanostructuring of polycrystalline metal films, *J. Phys.: Condens. Matter* 21 (2009) 224001.
- [21] Z. Pászti, G. Pető, Z. E. Horváth, O. Geszti, A. Karacs, L. Guzzi, Nanoparticle formation induced by low-energy ion bombardment of island thin films, *Appl. Phys. A* 76 (2003) 577–587.
- [22] V. Resta, R. J. Peláez, C. N. Afonso, Importance of ion bombardment during coverage of Au nanoparticles on their structural features and optical response, *J. Appl. Phys.* 115 (2014) 124303.
- [23] B. Satpati, P. V. Satyam, T. Som, B. N. Dev, Ion-beam-induced embedded nanostructures and nanoscale mixing, *J. Appl. Phys.* 96 (2004) 5212–5216.
- [24] S. Camelio, E. Vandenhecke, S. Rousselet, D. Babonneau, Optimization of growth and ordering of Ag nanoparticle arrays on ripple patterned alumina surfaces for strong plasmonic coupling, *Nanotechnology* 25 (2014) 035706.
- [25] S. Camelio, D. Babonneau, D. Lantiat, L. Simonot, F. Pailloux, Anisotropic optical properties of silver nanoparticle arrays on rippled dielectric surfaces produced by low-energy ion erosion, *Phys. Rev. B* 80 (2009) 155434.
- [26] Lumerical inc. (vancouver, canada), <http://www.lumerical.com/tcad-products/fdtd/>.
- [27] L. Simonot, D. Babonneau, S. Camelio, D. Lantiat, P. Guérin, B. Lamongie, V. Antad, In situ optical spectroscopy during deposition of Ag:Si₃N₄ nanocomposite films by magnetron sputtering, *Thin Solid Films* 518 (2010) 2637–2643.
- [28] A. Losquin, S. Camelio, D. Rossouw, M. Besbes, F. Pailloux, D. Babonneau, G. A. Botton, J.-J. Grefet, O. Stéphane, M. Kociak, Experimental evidence of nanometer-scale confinement of plasmonic eigenmodes responsible for hot spots in random metallic films, *Phys. Rev. B* 88 (2013) 115427.
- [29] T. T. Järvi, J. A. Pakarinen, A. Kuronen, K. Nordlund, Enhanced sputtering from nanoparticles and thin films: Size effects, *EPL (Europhysics Letters)* 82 (2008) 26002.
- [30] S. Zimmermann, H. M. Urbassek, Sputtering of nanoparticles: Molecular dynamics study of Au impact on 20 nm sized Au nanoparticles, *Int. J. Mass Spectrom.* 272 (2008) 91–97.
- [31] L. Yang, M. P. Seah, E. H. Anstis, I. S. Gilmore, J. L. S. Lee, Sputtering yields of gold nanoparticles by C₆₀ ions, *J. Phys. Chem. C* 116 (2012) 9311–9318.
- [32] M. Pellarin, C. Bonnet, J. Lermé, F. Perrier, J. Laverdant, M.-A. Lebeault, S. Hermelin, M. Hillenkamp, M. Broyer, E. Cottancin, Forward and backward extinction measurements on a single supported nanoparticle: implications of the generalized optical theorem, *J. Phys. Chem. C* 123 (2019) 15217–15229.
- [33] A. Girard, H. Gehan, A. Mermet, C. Bonnet, J. Lermé, A. Berthelot, E. Cottancin, A. Crut, J. Margueritat, Acoustic mode hybridization in a single dimer of gold nanoparticles, *Nano Lett.* 18 (2018) 3800–3806.
- [34] O. Pluchery, L. Caillard, P. Dollfus, Y. J. Chabal, Gold nanoparticles on functionalized silicon substrate under coulomb blockade regime: An experimental and theoretical investigation, *J. Phys. Chem. B* 122 (2018) 897–903.

- 590 [35] M. Song, D. Wang, S. Peana, S. Choudhury, P. Nyga, Z. A. Kudyshev, H. Yu, A. Boltasseva, V. M. Shalaev, A. V. Kildishev, Colors with plasmonic nanostructures: A full-spectrum review, *Appl. Phys. Rev.* 6 (2019) 041308.